Tech-Sphere Journal of Pure and Applied Sciences (TSJPAS)
A Subsidiary of Tech-Sphere Multidisciplinary International Journal (TSMIJ)
Vol 1, Issue 1, 2024 Publication Edition

Equilibrium, Kinetic and Thermodynamic Studies of an *Elaeis Guineensis* Fingers Biochar-Doped ZnO Nanoparticles prepared using Chemical Bath Deposition Technique

Ezekiel. Clinton Oroke[1*], Frank Ikenna Nwabue[2], Felix Sunday Nworie[3]
[1] Department of Science Technology, The Federal Polytechnic, Ado-Ekiti, PMB 5351, Ekiti State, Nigeria
[2] Department of Chemistry, Alex Ekwueme Federal University Ndufu-Alike Ikwo, Ebonyi State, Nigeria
[3] Department of Industrial Chemistry, Ebonyi State University, P.M.B 053, Abakaliki, Ebonyi State, Nigeria.
*Corresponding author's email: oroke_ec@fedpolyado.edu.ng

ABSTRACT

This study investigated the equilibrium, kinetics and thermodynamics of doping ZnO nanoparticles with biochar prepared from *elaeis guineensis* fruit bunch fingers using chemical bath deposition. The dopant and doped samples were characterized using Fourier transform infrared spectroscopy (FTIR), Raman spectroscopy, scanning electron microscope coupled with energy dispersive x-ray spectroscopy (SEM-EDX) and Brunauer–Emmett–Teller (BET) surface area analyzer. FTIR showed important functional groups such as $-NH_2$, and -OH which were instrumental to the successful doping. The doped sample showed a prominent Raman spectra peak at 412 cm^{-1}, indicating the wurtzite structure of ZnO NPs. EDX showed some important groups II-IV metals with Zn-O combination ratio of 1:2. SEM micrograph of doped sample showed homogeneous and flower-like images while the dopant presented porous and irregular-large particles. BET showed increase in surface properties such as specific surface area, pore volume and pore diameter for the doped sample with both samples having meso-pore diameters. Adsorption and kinetics studies indicated that the in-situ deposition on the doped ZnO NPs followed Langmuir and Pseudo-second order while thermodynamics showed that the process was spontaneous and endothermic. The study indicated that the biochar has potentials either as dopant or biosorbent in thin films or adsorption studies respectively, and also revealed that proper understanding of the mechanism of the deposition process is crucial for optimal film performance.

GRAPHICAL ABSTRACT

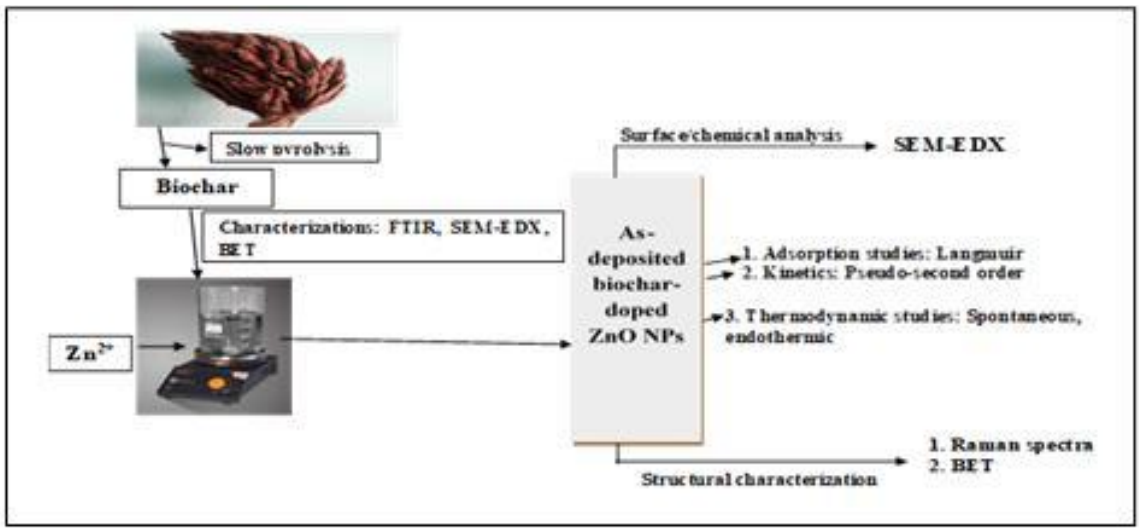

Keywords: Biochar-dopant, Adsorption, Kinetics, Thermodynamics, ZnO NPs.

1 Introduction

In the recent time, there has been significant surging scholarly interest geared towards the exploration of innovative materials and techniques aimed at the sustainable production of energy and combating environmental degradation. However, these techniques are not without challenges. Prominent amongst all the draw-backs faced by prevailing conventional efforts revolves around their deficiency to spontaneously integrate and degrade man-made waste [1]. Therefore, due to its unique innate nature and multidimensional usage, nano-materials have evolved as a pivotal strategy with considerable benign promise in various fields [2]. Nanoparticles has been considered as good candidate for these banes because of their miniaturize sizes (0 -100 nm), giving rise to large surface area for speedy reactions, better than in their bulk forms [3-4]. In addition, report has it that as material sizes become smaller, their energy bandgap are enhanced thus altering their optical, electrical and structural properties thus making them suitable for new device applications [4].

As a result, zinc oxide (ZnO) nanoparticles have attracted so many attentions due to its versatility as inorganic materials, broad bandgap (3.37 eV) and notably great exciton binding energy (60meV). These properties enhance their diverse range of applications across various fields of human endeavour [5-6]. According to Medhi *et al.* [7], doping induces alterations in the crystalline structure, surface characteristics, electronic properties, and more of the base metal, thereby boosting its potential applications.

There are various methods available for the deposition of films such as physical and chemical methods. Chemical method comprises of both gas and liquid phases such as chemical vapour deposition, atomic layer epitaxy, chemical bath deposition, spray pyrolysis, sol-gel, spin and dip coating respectively [8-9]. Among all these methods, chemical bath deposition (CBD) is most popular due to its simplicity, cost-effectiveness, tunability, robust and large surface deposition. It is the controlled growth of either metal sulfides, tellurides or oxides, usually in a basic medium, through ion-by-ion deposition on a glass substrate, resulting in the formation of films or nanoparticles as the case may be [9]. Its working principle is often dependent on the solubility of the product.

Elaeis guineensis is a multipurpose monocotyledonous plant that is widely grown for its oil-rich fruit bunches [10]. As a versatile plant, almost all its aspects have various economic applications except for the empty fruit bunch fingers. Biochar, otherwise known as a carbonaceous material sourced from biomass, is fabricated through the pyrolysis of solid waste at relatively low temperatures under either anoxic or anaerobic conditions [11 – 12]. Considering its remarkably porous nature, interest on biochar has tripled as a substrate for the development of functionalized, cheap biosorbent composite materials for the elimination of obnoxious elements or substances [12]. The inherent characteristics of biochar, such as raw material availability, economic viability, substantial specific surface area and pore volume, structural stability, abundant active functional groups, and high adsorption strengths have further increased research interests both for adsorption and as a dopant in thin film studies [11].

Since the advent of thin film studies, a variety of metals and a few biomaterials have been explored as dopants. However, despite some drawbacks associated with using metals, there is limited understanding regarding the impact of using biowaste as a dopant material in ZnO quantum dots [13 – 18]. Additionally, questions concerning the specific mechanisms by which biowaste and or metals influences the synthesis, together with the resultant optical, electronic, and structural properties of the quantum dots, have remain unanswered. Studying the mechanisms of thin film deposition, which is synonymous to adsorptions studies could provide crucial insights into the interactions, reaction rates, and stability of the nanomaterials and ultimately facilitating their practical applications of the films in environmental and energy-related fields.

Therefore, this study is aimed at providing a thorough understanding of the process of doping the prepared *elaeis guineensis* biochar on ZnO nanoparticles by probing into the various equilibrium, kinetic, and thermodynamic mechanisms of their synthesis.

2 Experimental Procedure

Reagents employed in this investigation were all analytical standard most of which were sourced from Sigma Aldrich®, USA. They were therefore utilized without additional purification unless specified otherwise, with distilled water being consistently used throughout the study.

2.1 Sample Collection and Preparation

The Federal Polytechnic Ado-Ekiti Oil Palm Plantation Reserve provided the oil palm (*elaeis guineensis*) fruit bunch fingers utilized in the production of the biochar [16]. The bunch fingers were first cleaned with distilled water to eliminate contaminants and then air-dried under sunlight for 24 hours to eliminate moisture. Samples of the *elaeis guineensis* fingers was taken to the Forestry Research Institute of Nigeria, Ibadan for identification and was assigned voucher number F101173 in the Institute's herbarium.
The sample was subsequently introduced into the furnace, which had been hitherto cleaned with distilled water to avert contamination while allowing a residence time of 20 minutes at 200 ±1°C in a limited oxygen. The resulting product was then retrieved, cooled, weighed and particle size reduced with the aid of laboratory mortar and piston; sieved with a micro-sieve (0.137 mm) to achieve desired sizes, and then preserved in a desiccator for subsequent analysis [17 – 18].

2.2 Ligand synthesis

(4,4'-(1, 2-ethanediyldinitrilo)bis-(2-pentanone)), code-named as EDDBP was used as ligand for the study. It was synthesized following a method outlined in [19]. The standard solution of the ligand ($C_{12}H_{20}N_20_2$) was then prepared by dissolving 0.5 g in 20 mL distilled water and adjusting the volume to 100 mL

2.3 Synthesis of The Doped-ZnO Nanoparticles

The in-situ as-deposited doped-ZnO NPs were deposited onto a matched silica glass substrate, which had been prepared using a method adapted from previous reports [20 – 22]. The bath composed of 10 mL each, of 0.1 M $ZnSO_4.7H_2O$ (Sigma-Aldrich®, USA, 99%), 0.2 M NaOH (Sigma-Aldrich®, USA, 97%,) and 5 mL of the ligand (EDDBP) respectively. The solution was attuned to round up the strength of the ions in bath to 0.1 M, pH range of 8 to 12 with NH_4Cl (0.02 M), while adding 28% NH3 and HCl drops. The bath volume was thereafter adjusted with distilled water to 100 mL. The matched substrates were gently immersed in the solution and agitated at 300 rpm while varying the conditions as needed. After a fixed duration, the slide was withdrawn, rinsed with distilled water (5 mL), air-dried for 1 h, and stored in a desiccator subsequent analysis. The possible formation process for the synthesis of the doped-ZnO NPs at pH 10 are represented in equation 1 - 3:

$$ZnSO_4.7NaOH \rightarrow Zn(OH)_2 + Na_2SO_4 + 7H_2O \quad \text{.....1}$$

$$Zn(OH)_2 + 2OH \rightarrow [Zn(OH)_4]^{2-} \quad \text{.....2}$$

It is possible that a monodentate functional group present in the biochar can coordinate with Zn displacing one hydroxyl (-OH) from $[Zn(OH)_4]^{2-}$ which eliminates one mole H_2O and OH^- to form the doped ZnO

$$[Zn(OH)_3 - BC]^- \rightarrow ZnO - BC_{\downarrow} + H_2O + OH^- \text{……..……..3}$$

2.4 Characterization of the dopant and the synthesized doped NPs

Prior to conducting characterizations with equipment; pH of the biochar was evaluated with the aid of a high sensitive digital pH meter and was found to be 8.2.

Microstructural, surface morphological as well as textural properties of both the biochar and doped ZnO nanoparticles were analyzed using several techniques. These included Fourier transform infrared spectroscopy (FTIR) (Agilent Technologies), Raman spectroscopy (model: ProRaman-L-785-BIS Ser.No.196166, with wavelength of excitation of 514 nm and laser power of 1.5 mW), SEM-EDX (model Phenom ProX, by PhenomWorld Eindhoven, The Netherlands), while specific surface area was analyzed through N_2 adsorption/desorption employing Brunauer-Emmett-Teller (BET) method.

2.5 Equilibrium, kinetics and thermodynamic studies

It is important to examine the adsorption equilibrium data with focus on different isotherm models which serves as a crucial initial stage in identifying a proper model for designing a process [23]. Consequently, modeling of data obtained from equilibrium from adsorption processes holds significant importance in adsorption mechanisms projection across different systems. This helps in understanding the adsorbent's surface properties and adsorptive capacity. To investigate the behaviour and mechanisms of the biochar-doped as-deposited ZnO NPs under varying conditions, Langmuir, Freundlich, Temkin, and Elovich equilibrium isotherms were employed.

Data collected during the study, including film thickness, were subjected to analysis using pseudo-first and second-order kinetics, together with Weber-Morris models to forecast the kinetics and also identify the rate-limiting step of the deposition process. The coefficient values of regression at each stage validate the appropriateness of using the model to test the deposition process [24].

Furthermore, the influence which variation in temperature could have on the deposition of Zn^{2+} onto biochar was studied temperature ranges of 30 to 100^{o}C at initial Zn^{2+} concentration of 0.01–0.1 Mol/100 mL, while keeping the biochar concentration constant at 1 g/100 mL and an optimal pH of 10. This aspect of the study was conducted using thermodynamic parameters, standard enthalpy, entropy, and Gibbs free energy.

3 Results and Discussion

3.1 FTIR characterization

This was done to identify various important function groups and phytochemicals available both in the dopant and the as-deposited doped-ZnO Nanoparticles as was shown in Table 1.

From Table 1, the biochar exhibited prominent vibrational bands. A significant peak which is linked to alcohol (-OH stretching) was seen at 3678.9 cm^{-1}. A distinct band at 3281.4 cm^{-1} characterized the amines in the samples. The Sp^3 stretching of alkanes and the medium intensity C≡C stretching of alkynes, respectively, are represented by the noticeable bands found at 2922.2 cm^{-1} and 2109.7 cm^{-1} [25] The stretching of isothiocyanate (N=C=S) together with the N-H bending of the amines were also revealed by broad bands detected at 1919.6 cm^{-1} and 1580.4 cm^{-1} respectively. Stretching, as well as medium bending synonymous to the bands of vinyl ester, sulphoxide (S=O), and 1,2,4-trisubstituted alkane were indicated by other lesser peaks at 1376.4 cm^{-1}, 1218.8 cm^{-1}, 1036.2 cm^{-1}, and 872.2 cm^{-1} respectively. Various reports

have indicated that nitrogen-containing active sites and O-H group boosts the surface alkalinity of biochar, thus enhancing it applicability in CO_2 removal, as ligand and or stabilizing agent [1, 25-26]. According to [1], hydroxyl and amino active sites are crucial in expelling Cr(VI) and other harmful obnoxious metals from environment. The band seen at 2922 cm^{-1} suggests sp^3 hybridization.

Comparing the biochar with the doped-ZnO NPs, it showed a reduction in bands as was noted in the spectra of the later. There was an observable loss of two significant bands (Table 1) assigned to alcohols and amines. Possible reasons as regards the reduction in absorption band to shorter wave numbers has previously been reported [27]. Consistent with report of [28], the same band seen at 2922.2 cm^{-1} in the biochar spectra, was also detected in the synthesized nanoparticles. Weak bands were noticed within fingerprint regions (Table 1), which is linked to -C-O stretching of ethers and the -C-H bending of metal-replaced aryl compounds respectively. According to earlier reports, majority of metal-oxides show their stretching vibrations within bands < 1000 cm^{-1}, with the distinctive peak of ZnO typically observed at 416 cm^{-1} [24, 26]. As a result, the faint band at 752.9 cm^{-1} could be ascribed to the minor amounts of Zn-O bonding.

Table 1: FTIR results for the biochar and the as-deposited biochar doped ZnO nanoparticles

Identity of sample	Absorption (cm^{-1})	Intensity	Designation	Class of compound
	3678.9	S	O-H Stretching	Alcohols
	3281.4	S	N-H Stretching	Amines
	2922.2	S	C-H	Alkanes
	2109.7	M	C≡C	Alkynes
	1919.6	S	N=C=S Stretching	Isothiocyanate
FB_fBC	1580.4	S	N-H Bending	Amine
	1376.4	M	CH3 Bending	Alkane
	1218.8	S	C-O	Vinyl ester
	1036.2	S	S=O	Sulphoxide
	872.2	M	C-H bending	1,2,4-trisubstituted
	2922	S	C-H	Alkanes (SP3)
	2855.1	S	C-H Stretching	Alkanes
	2325.9	S	O=C=O	Carbon (iv) oxide
	2165.6	M	C≡C	Alkynes
ZnO-FBfBC	1997.9	S	N=C=S Stretching	Isothiocyanate
	1744.4	S	C=O	5-membered cyclic ketone
	1457.4	M-S	C=C Stretching	Aromatic compound
	879.7	S	C-O Stretch	Ethers
	752.9	S	C-H Bend	m-disubstituted aromatic compound

3.2 Raman Analysis

Figure 1 is the Raman spectra of biochar-doped ZnO NPs deposited pH of 10, and wavenumber spanning from 0 – 3000 cm^{-1}. The findings showed a zero defect intensity peak, otherwise known as the D-band, in

the doped sample. This absence suggests lack of ring breathing mode which is associated with sp^2 carbon rings in the samples, suggesting a multi-walled or layered structure. This result further validates the FTIR report for doped NPs. According to [29], such multilayered semiconductors exhibits unique properties from their bulk counterparts, thus making them promising candidates for integration into electronic circuits.

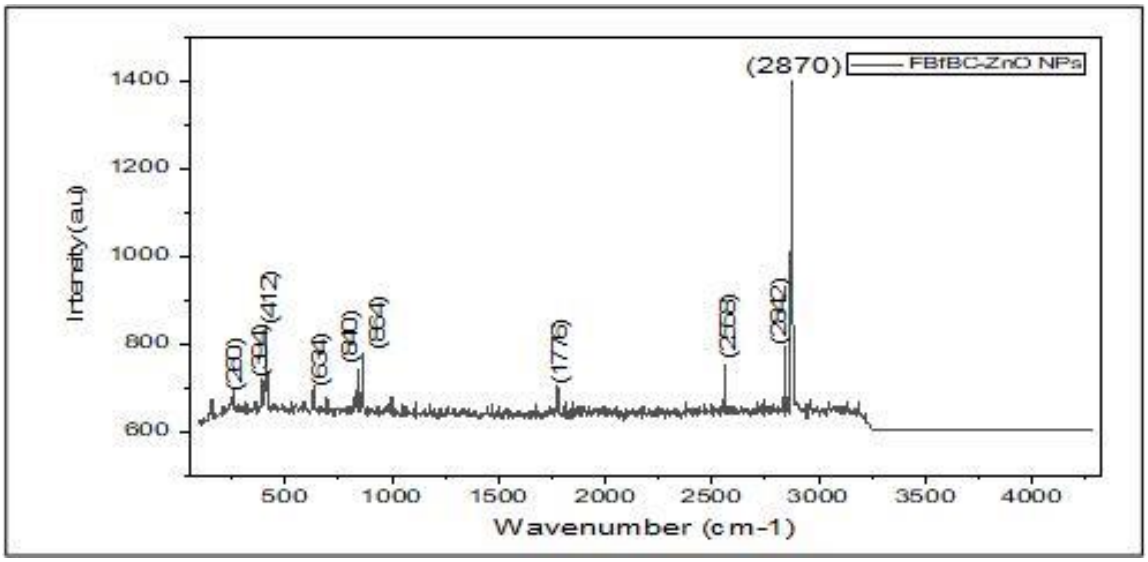

Figure 1: Raman spectral bands of the Biochar-doped ZnO NPs at pH 10

Additionally, the biochar-doped sample displayed a considerable hypsochromic shift from the G-band, for as high as 194 cm^{-1}, as well as multiple 2D-bands which surpassed standard values, at ~172 cm^{-1} (typically 1582 and 2700 cm^{-1}) [30]. This regular peak shift in either the G or 2D-bands is linked to straining which may have been triggered-off by the glass substrate during the transfer process of ZnO-biochar films [28, 30]. Although, 2D-band arises from a two-phonon lattice vibrational mechanism, contrary to D-band; proximity to a defect is not always necessary for its activation. It is a prominent spectral feature associated with graphene, frequently observed even in samples lacking a D-band, and its presence does not necessarily signify the presence of defects.

Consistent to the report of [31], Raman spectral peaks from 150 – 430 cm^{-1} are commonly attributed to metal oxides. There was a prominent peak at 412 cm^{-1} for the doped sample. Significant bands around 436 cm-1 is a known feature of ZnO with wurtzite E_{2high} mode which most times shifts towards shorter wavelengths when it comes to nanoparticles. This phenomenon arises as a result of anisotropic internal strains associated with various growth directions, impurities within the nanocrystals and or as a result of optical phonon confinement within distinct nanostructures [26, 32 – 33].

3.3 Elemental Study

To investigate the elemental composition and their combination ratio in both dopant and the doped ZnO nanoparticles, EDX was employed. Figures 2 a and b as well as table 2 shows the composition of elements in both samples.

It could be seen from the Table 2 both samples have significant elements such as potassium, calcium, silicon, aluminium together with other groups IV to VI elements. Notably, EDX results showed reasonable amounts of elements like carbon, chlorine, in addition to titanium in the biochar and the doped ZnO nanoparticles respectively.

Examination of the doped sample revealed that the ratio of combination of Zn to O is 1:2, with Zn having 5.56 while oxygen had 12.02. The decreased concentration of Zn may likely be connected to flaws created by the metallic elements in the biochar, which may have displaced Zn^{2+} by entering into its lattice. This may be likely as a result of differences in periodic properties of the elements present in the biochar [34]. Additionally, large concentration of Si seen in the FB_fBC- ZnO NPs (Fig. 2b and table 2) may be attributed to the substrate employed in this investigation

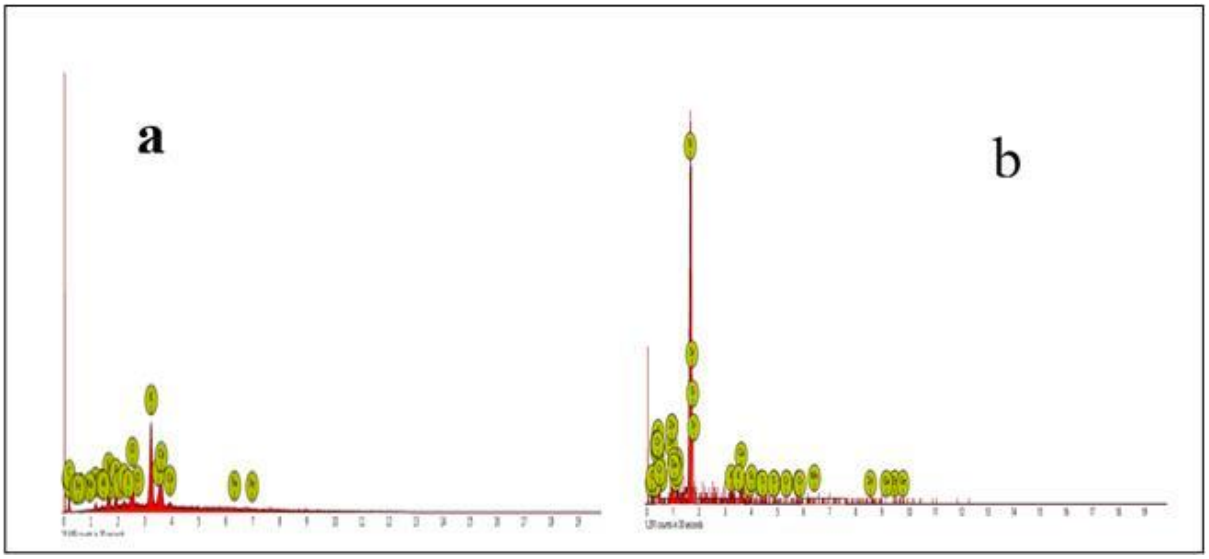

Figure 2a and b: EDX spectra of the biochar and the FB_fBC-ZnO NPs

Table 2: Composition of elements of the dopant and FBfBC- ZnO NPs

Element No		**Symbol**	**Name**	**Sample and weight conc.**	
				FB_fBC	**FB_fBC- ZnO**
19		K	Potassium	39.81	0.54
6		C	Carbon	24.14	4.65
20		Ca	Calcium	15.92	4.73
17		Cl	Chlorine	10.64	ND
14		Si	Silicon	3.91	28.79
15		P	Phosphorus	3.04	ND
16		S	Sulphur	1.75	ND
12		Mg	Magnesium	1.05	1.28
13		Al	Aluminium	0.25	ND
8		O	Oxygen	0.01	12.02
11		Na	Sodium	0.00	4.88
26		Fe	Iron	0.00	ND
47		Ag	Silver	ND	ND
30		Zn	Zinc	ND	5.56

22		Ti	Titanium	ND	0.64
25		Mn	Manganese	ND	1.59
31		Ga	Gallium	ND	1.42
38		Sr	Strontium	ND	20.03
23		V	Vanadium	ND	0.94
24		Cr	Chromium	ND	0.65
21		Sc	Scandium	ND	1.26
32		Ge	Germanium	ND	11.01

Where ND = Not Detected

.

3.4 Surface morphological characterization

Figures 3a and b are SEM micrograph of FB_fBC-ZnO NPs and FB_fBC. Figure 3a indicates that the deposited film manifested a nano-flower (NF) morphology with zero voids. Furthermore, it displayed a homogeneous, fine and crack-free morphology with grains which are regularly spread with tiny pinholes. The present report is consistent with the findings by [35] and [11], thus affirming the nano-structural characteristics of the doped ZnO.

In contrast, Figure 3b revealed numerous ordered but relatively irregular large shapes characterized by visible pores [36]. The porous nature displayed diverse shapes and scales of both meso and macropores, possibly as a result of the presence of volatiles retained during low-temperature carbonization [37].

Meso and macroporous particles have been reported to be very important in adsorption of hazardous contaminants in aqueous media [38]. Therefore, due to its porous nature, vascular bundles, and internal pore structure, the biochar presents itself as a potential economical adsorbent for the elimination of recalcitrant obnoxious contaminants in aqueous solutions. Similarly, its innate centers of attachment boosts its suitability for utilization as dopants in semiconductor thin film research [39].

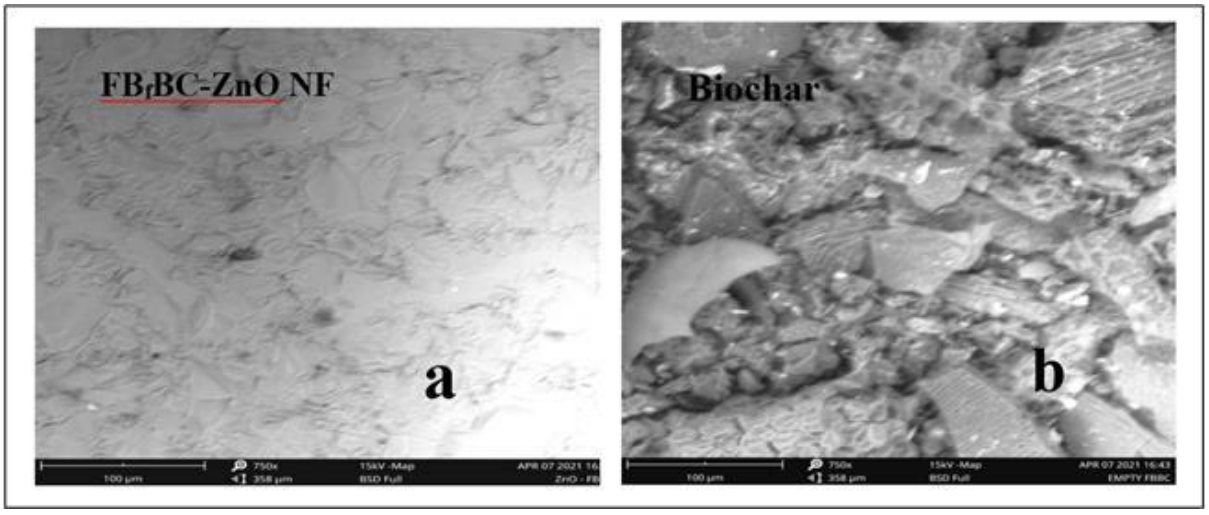

Figure 3a and b: SEM images of the FB_fBC -ZnO NF and the oil palm fingers biochar

3.5 Textural Characterization

The textural characteristics of the biochar as well as the doped sample were analyzed through nitrogen adsorption analysis employing the BET surface area method [40]. The surface area per unit mass, void volume and pore width of both samples are presented in Table 3.

Results indicated that the dopant's surface area per unit mass, void volume and pore width were respectively 155.195 m^2/g, 0.077 cc/g, and 2.141 nm. On the other hand, these properties increased for the doped ZnO nanoparticles to 200.797 m^2/g, 0.097 cc/g, and 2.207 nm. According to reports, one major function of biochar are raising the surface area and functional sites in metal oxide nanoparticles [41, 34]. This report agrees with the work of [42].

Comparing this work with similar studies, surface characteristics obtained in this investigation were notably greater [39, 43]. The improvement in surface area and mesoporous pore diameters in both samples signify advantageous features suitable for the elimination of environmental pollutants, as they enhance photocatalytic activity [34].

Table 3: BET result of surface characteristics of biochar and the doped ZnO- FB_fBC nanoparticles

Sample identity	Surface area per unit mass (m^2/g)	Void volume (cc/g)	Pore width (nm)
FB_fBC	155.195	0.077	2.141
ZnO-FB_fBC	200.797	0.097	2.207

3.6 Adsorption Isotherms

3.6.1 Adsorption Isotherms

This was applied to forecast the effectiveness of various biosorbents. The model rests on the presumption that adsorption occurs on uniform sites, terminating immediately all sites are occupied, with no interaction between adsorbate molecules on neighbouring sites. Equation 4 is a linear representation of the Langmuir isotherm [44 – 46].

$$\frac{Ce}{qe} = \frac{\mathrm{Ce}}{Qm} + \frac{1}{bQm} \quad \ldots\ldots 4$$

Here, equilibrium amount of the biochar-ZnO NPs is represented with Ce (mg/g), while the quantity of biochar is denotes with qe (mg/g). Parameters such as Qm and b stands for Langmuir constants, which respectively the highest adsorption capacity and energy of bonding. From figure 4, factors Qm and b were derived as slope and intercept respectively by plotting Ce/qe versus Ce and estimated to be 20 and 1.6 x 10^{-5}.

In order to estimate the dimensionless separation factor, which measures the workability and favourability of the isotherm, the Langmuir parameter b, was utilized, see equation 5.

$$R_L = \frac{1}{1+\mathrm{bCo}} \quad \ldots\ldots 5$$

While Co denotes Zn^{2+}original amount, b represents Langmuir constant and R_L is a separation factor which determines if the model will be linear, feasible or not. Therefore, when the value of $R_L = 1$, it indicates linearity; R_L greater than 1 implies non-feasibility/viability, whereas $0 < R_L < 1$ suggested the viability of adsorption/deposition process.

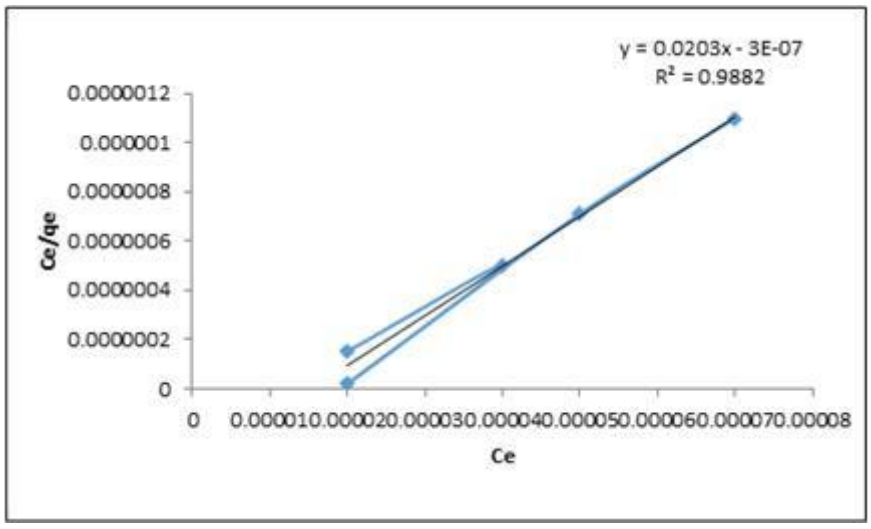

Figure 4: Langmuir model for the doped-ZnO NPs at optimized conditions

3.6.2 Freundlich isotherm

This considers kinetics of a multilayer adsorption process on an adsorbent. The model holds that adsorbent's surface is heterogeneous, while binding-site's active energies are exponentially distributed. Here, adsorption proceeds pending when the heat of adsorption drops in an exponential order as the process approaches completion [47]. Equation 6 is the mathematical representation of the Freundlich isotherm while its linear form is as shown in equation 7 [48 - 49, 44].

$$qe = KFCe^{\frac{1}{n}} \quad \ldots\ldots\ldots\ldots\ldots\ldots\ldots\ldots\ldots\ldots\ldots\ldots\ldots\ldots\ldots\ldots\ldots\ldots\ldots\ldots\ldots\ldots 6$$

$$Inqe = InKf + \frac{1}{n}InCe \quad \ldots\ldots\ldots\ldots\ldots\ldots\ldots\ldots\ldots\ldots\ldots\ldots\ldots\ldots\ldots\ldots\ldots\ldots\ldots\ldots\ldots\ldots 7$$

With n standing for adsorption intensity, K_F denotes the dopant's capacity to adsorb derived as intercept and slope respectively in Figure 5.

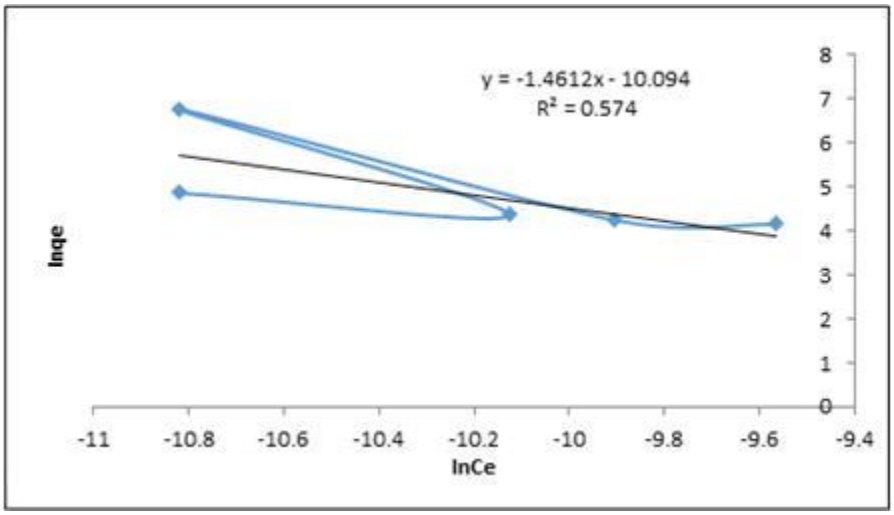

Figure 5: Freundlich model for the doped ZnO at optimized conditions

3.6.3 Elovich isotherm

This postulates that surfaces of actual adsorbents are heterogeneous in terms of energy. It is centered on the multilayer adsorption concept, with extent of adsorption increasing exponentially as long as there are available adsorption sites [47]. Figure 6 is a graph of ln(qe/Ce) against qe which gave an R^2 value of 0.836. This value is lesser than the R^2 values obtained for the Langmuir isotherm but higher than those for the Freundlich and Temkin models, therefore suggesting that the adsorption/deposition is a monolayer bio-doping. Equation 8 is the linear representation of Elovich isotherm.

$$\frac{qe}{qm} = \mathrm{KECe}^{\frac{qe}{qm}} \quad \text{.....8}$$

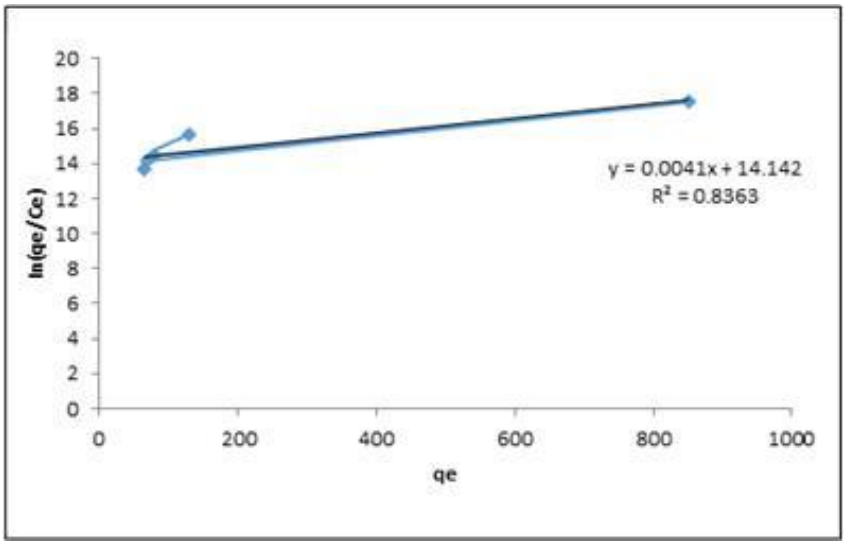

Figure 6: Elovich model for the doped-ZnO NPs at optimized conditions

3.6.4 Temkin model

This is mostly employed for a sorbate that is intermediary. According to [44], Temkin isotherm postulates that there is a decrease in the heat accompanying molecules' adsorption within the layer diminishes linearly with the coverage area due to sorbent-sorbate interactions, rather than following a logarithmic relationship. Linear relationship of this isotherm is represented in equation 9.

$$q_e = \beta \mathrm{In}A_t + \beta InC_e \quad 9$$

While β represents sorption heat, A denotes adsorbate- adsorbent binding constant at equilibrium. At and β were obtained from the graph of qe versus InCe slope and intercept respectively. The R^2 value obtained from the plot (Fig. 7) was 0.397; a value that is far lower than those of other isotherms.

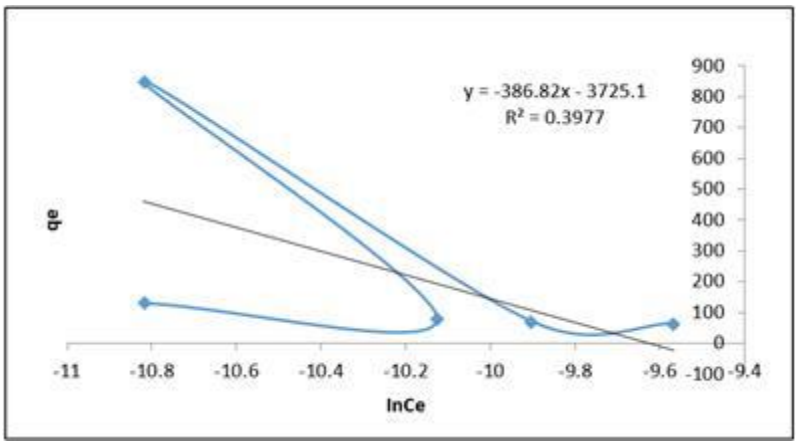

Figure 7: Temkin isotherm for the doped ZnO NPs at pH 10, 303± 1K

From figures 4 – 7 and considering the R^2 values of the isotherm models examined, it clearly indicate that the adsorption was monolayer thus suggesting that the biochar doping closely followed the Langmuir adsorption isotherm. This further submits that sites for adsorption are identical energetically, equivalent, homogeneous structurally, without significant interface between the adsorbed molecules and adjacent sites. This implies that the transfer of adsorbate between available sites is almost impossible, and the biochar has a discrete capacity for the adsorption for Zn^{2+}. In addition, an R_L value of 0.0004, which falls within the range $0 < R_L < 1$, suggests that the deposition process is favourable.

3.7 Kinetic Models

3.7.1 Pseudo-First and Second Order kinetics

Equations 10 and 11 are linear expressions of Lagergren pseudo-first and second order kinetics equations which were employed to study the kinetics of the whole process [50, 48, 45].

$$\mathrm{Log(qe - qt)} = Logqe - (\frac{K1}{2.303})t \quad \ldots\ldots 10$$

$$\frac{\mathrm{t}}{\mathrm{qt}} = \frac{1}{K2}qe^2 + t/_{qe} \quad \ldots\ldots 11$$

The symbols qe and qt, respectively, indicate the concentration (mg/g) of ZnO-BC deposited at any other time, t as well as equilibrium time. Figure 8 and 9 are plots of log (qe - qt) against t, and t/qt versus t and from where rate constants (K_1 and K_2) for pseudo-first and second order models respectively, were evaluated.

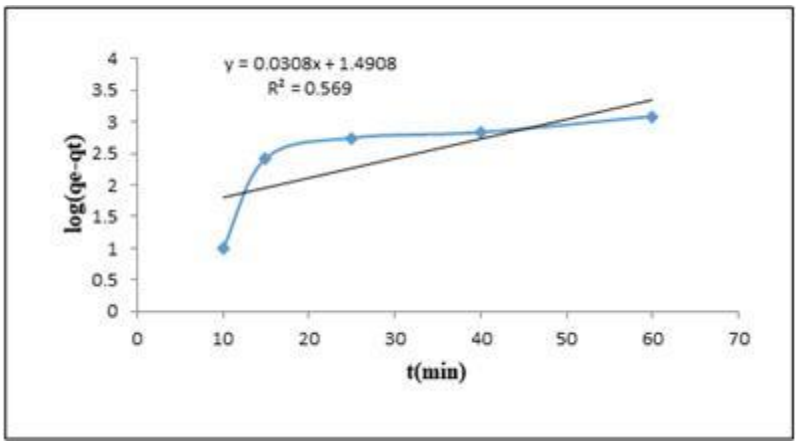

Figure 8: Pseudo first-order kinetics of BC-ZnO NPs at pH 10, 303± 1K

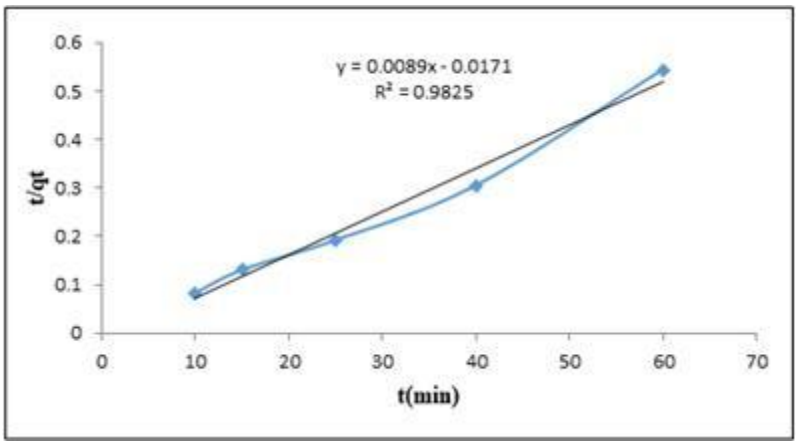

Figure 9: Pseudo second-order kinetics of BC-ZnO NPs at pH 10, 303± 1K

3.7.2 Weber-Morris intra-particle model

Intra-particle diffusion model, represented by equation 12, characterizes the adsorption process in which there is proportional variation of solute sorption with $t^{1/2}$ rather than t. As a result, for intra-particle diffusion to be the rate-limiting step in the deposition process, graph of qt versus $t^{1/2}$ must yield a straight line passing through the origin while Ki and C stands for slope and intercept, respectively. Equation 12 is the linear relation of the model.

$$qt = K_i t^{1/2} + C \quad \ldots\ldots 12$$

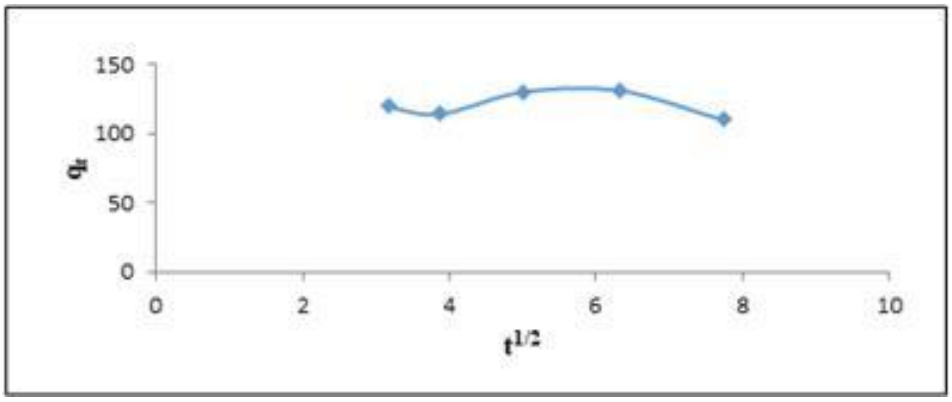

Figure 10: Weber-Morris Intra-particle model for the doped-ZnO NPs at pH 10, 303± 1K

Applying kinetic models to information obtained in this study, pseudo-first-order (Fig. 8) gave a low R^2 value of 0.569 and a K_1 of 1.50, while the pseudo-second-order kinetics (Fig. 9) displayed R^2 and K_2 values of 0.982 and 0.025 respectively. From the results, it is clear that the process did not follow pseudo-first-order kinetics but aligns well with the pseudo-second-order kinetics. In this model, reactions are driven by chemisorption, which, in other words; determines the rate-limiting step. Therefore, the results indicates an equal rate of reaction with the adsorbent-surface's number of functional sites [48, 51]. Hence, the deposition was primarily a chemisorption process.

From the result (Fig. 10), it is suggestive that the deposition processes was not prompted by intra-particle diffusion of the films since it neither showed a straight line nor passed from the origin rather, was controlled by kinetic order as the rate-limiting step [49, 52].

3.7.3 Thermodynamic Studies

When evaluating rate of chemical reaction adsorption processes, temperature is an important factor [43]. Equations 13 – 16 shows thermodynamic parameters.

$$Kc = \frac{CAe}{Ce} \quad \text{.....13}$$

$$\Delta G^o = -RTInKc \quad \text{..... 14}$$

$$\Delta G^o = \Delta H^o - T\Delta S^o \quad \text{.....15}$$

$$LogKc = \frac{\Delta So}{2.303R} - \frac{\Delta Ho}{2.303RT} \quad \text{.....16}$$

The acronym CAe stands for the concentration of Zn^{2+} trapped on the surface of the adsorbent per liter of solution at equilibrium, whereas Kc stands for the equilibrium constant and Ce for equilibrium quantities in solution (All in mg/L). A plot of log Kc against 1/T (Fig. 11) was used to estimate ΔH^o as well as ΔS^o in terms of slope and intercept.

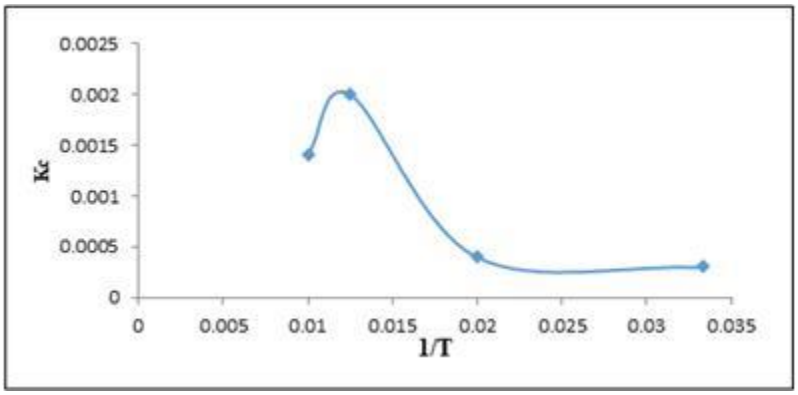

Figure 11: Thermodynamic properties of the doped-ZnO NPs at 30 – 100 oC, pH 10

Oftentimes, evaluation of the attributes of thermodynamics in adsorption studies are interpreted in terms of exothermic or endothermic processes. Consequently, three major factors, including Gibbs free energy (ΔG°), enthalpy (ΔH°), and entropy (ΔS°) are mostly utilized. ΔH° results that indicated positivity (1.56 x 10^{-4} Kjmol) and ΔS° (2.75 x 10^{-2} Jmol/K) suggested that the process was endothermic in nature. Furthermore, negative ΔG° (-8.33Kjmol) value confirmed that the process was feasible and spontaneous [23, 45].

Evaluation of the thermodynamic properties in adsorption research is often explained in terms of endothermic or exothermic processes. As a result, the most primarily used parameters are entropy (ΔS°), enthalpy (ΔH°), and Gibbs free energy (ΔG°). The deposition was determined to be endothermic based on the positivity of ΔH° (1.56 x 10^{-4} Kjmol) as well as ΔS° (2.75 x 10^{-2} Jmol/K). Moreover, the process was established as viable and spontaneous due to the negative ΔG° value (-8.33Kjmol) [23, 45].

4 Conclusions

Biochar prepared from *elaeis guineensis* by slow pyrolysis was used as dopant to prepare zinc oxide nanoparticles using in-situ chemical bath deposition technique. Data obtained in the study such as film thickness, was employed in investigating the equilibrium, kinetics and thermodynamics of the process. Characterization of both samples were done to unravel their structural, surface morphological as well as chemical properties using FTIR, Raman spectroscopy, SEM-EDX and BET surface area analyzer respectively. Results as shown by FTIR indicated the presence of important functional groups which aided the successful deposition while Raman spectra of the doped sample confirmed the wurtzite phase of ZnO NPs showing that the deposition was multi-walled. Surface topography of the doped sample showed the presence nano-flower while EDX indicated a Zn-O combination ratio of 1:2. Moreover, BET showed that there was increase in surface area of the doped sample and also confirmed its mesoporous nature. Adsorption equilibrium as well as kinetics established that the deposition agreed with Langmuir model and pseudo-second-order whereas thermodynamic examination indicated their spontaneous and endothermic nature. This study generally exposes the importance of studying the adsorption mechanism of thin film deposition and some useful properties of biochar prepared from *elaeis guineensis*.

.

5 Declarations

Data supporting the findings in this study are available from the corresponding author upon reasonable request.

5.1 Acknowledgements

Authors appreciate the efforts of Mr. Isa Yakubu, Technologist in the Department of Chemical Engineering, Ahmadu Bello University (ABU), Zaria-Nigeria, Mr. Abdulkareem Bello of Biotechnology Research laboratory, Federal University of Technology, Minna Niger State respectively, for availing us the required equipment to embark on this research. We appreciate the Staff of the Central Research Laboratory, Federal Polytechnic Ado Ekiti, for assistance in other equipment that was used in this study.

5.2 Funding source

Not applicable.

5.3 Competing Interests

Authors wish to declare that there is no relevant financial, non-financial or personal interests that could have influenced or influenced the results reported in this paper.

References

[1] Zhang Q, Suresh L, Liang Q, Zhang Y, Yang L, Paul N, Tan SC (2021) Emerging Technologies for Green Energy Conversion and Storage. Advanced Sustainable System 5(3): 2000152.

[2] Muhammad S, Muhammad I, Chanbasha B, Madiha T, Muhammad D, Nadeem B, Farrukh S (2015) Impact of nanoparticles on human and environment: Review of toxicity factors, exposures, control strategies and future prospects. Environ. Sci. Pollut. Res 22: 4122 - 4143.

[3] Jing H, Ji L, Wang Z, Guo J, Lu S, Sun J, Cai L, Wang Y (2021). Synthesis of ZnO Nanoparticles Loaded on Biochar Derived from Spartina alterniflora with Superior Photocatalytic Degradation Performance. Nanomaterials 11: 2479.

[4] Devi PG, Velu AS (2016) Synthesis, structural and optical properties of pure ZnO and Co doped ZnO nanoparticles prepared by the co-precipitation method. J Theor Appl Phys 10:233–240

[5] Ngoepe NM, Mbita Z, Mathipa M, Mketo N, Ntsendwana B, Hintsho-Mbita NC (2018) Biogenic synthesis of ZnO nanoparticles using Monsonia burkeana for use in photocatalytic, antibacterial and anticancer applications. Ceramic International 44(14):16999 – 17006.

[6] Saboor A., Shah S. M., Hussain H (2019) Band gap tuning and applications of ZnO nanorods in hybrid solar cell: Ag-doped verses Nd-doped ZnO nanorods. Materials Science in Semiconductor Processing, 93: 215 - 225.

[7] Medhi R, Marquez MD, Lee TR (2020) Visible-Light-Active Doped Metal Oxide Nanoparticles: Review of their Synthesis, Properties, and Applications. ACS Appl. Nano Mater 3: 6156–6185.

[8] Chaudhari MN, Ahirrao RB, Bagul SD (2021) Thin film Deposition Methods: A Critical Review. International Journal for Research in Applied Science & Engineering Technology (IJRASET). 9(6)

[9] Kumar, KDA, Valanarasu, S, Rosario SR, Ganesh V, Shkir M, Sreelatha CJ, AlFaify S (2018) Evaluation of the structural, optical and electrical properties of AZO thin films prepared by chemical bath deposition for optoelectronics. Solid State Sciences doi: 10.1016/j.solidstatesciences.2018.02.003.

[10] Onakurhefe P, Achuba FI, George BO, Okpoghono J (2020) Effect of Elaeis guineensis (Jacq) leaf extracts on crude oil-induced genotoxicity in Wistar albino rats. Scientific African 7 (2020) e00280 https://doi.org/10.1016/j.sciaf.2020.e00280

[11] Sun Y, Yu F, Han C, Houda C, Hao M, Wang Q (2022) Research Progress on Adsorption of Arsenic from Water by Modified Biochar and Its Mechanism: A Review. Water 14: 1691.

[12] Zhou Y, Gao B, Zimmerman AR, Cao X (2014) Biochar-supported zerovalent iron reclaims silver from aqueous solution to form antimicrobial nanocomposite. Chemosphere 117: 801.

[13] Hancock JM, Rankin WM, Hammad TM, Salem JS, Chesnel K, Harrison RG (2014) Optical and Magnetic Properties of ZnO Nanoparticles Doped with Co, Ni and Mn and Synthesized at Low Temperature. Journal of Nanoscience and Nanotechnology 15:(5): 3908 -3815.

[14] Akcan D, Ozharar S, Ozugurlu E, Arda L (2019) The effects of Co/Cu Co-doped ZnO thin films: An optical study. Journal of Alloys and Compounds 797: 253-261.

[15] Akhil K, Jayakumar K, Gayathri G, Khan SS (2016) Effect of various Capping agents on Photocatalytic, Antibacterial and Antibiofilm activities of ZnO Nanoparticles. Journal of Photochemistry and Photobiology, B: Biology, 2016;160: 32 - 41.

[16] Alsaad A. M., Al-Bataineh Q. M., Ahmad A. A., Albataineh Z., Telfah A (2020) Optical band gap and refractive index dispersion parameters of boron-doped ZnO thin films: A novel derived mathematical model from the experimental transmission spectra. Optik - International Journal for Light and Electron Optics 211:164.

[17] Devi KR, Selvan G, Karunakaran M, Kasirajan K, Chandrasekar LB, Shkir M, AlFaify S (2020) SILAR-coated Mg-doped ZnO thin films for ammonia vapor sensing applications. Journal of Materials Science: Materials in Electronics 31(5): 10186–10195.

[18] Dananjaya SHS, Kumar RS, Yang M, Nikapitiya C, Lee J, De Zoysa M (2018) Synthesis, Characterization of ZnO-chitosan Nanocomposites and Evaluation of its Antifungal activity against Pathogenic Candida albicans. International Journal of Biological Macromolecules 108: 1281-1288.

[19] Usman ARA, Abduljabbar A, Vithanage M, Ok YS, Ahmad M, Ahmad M, Elfaki J, Abdulazeem SS, Al-Wabel MI (2015) Biochar Production from Date Palm Waste: Charring Temperature Induced changes in composition and Surface Chemistry. Journal of Analytical and Applied Pyrolysis 115: 392 - 400.

[20] Adeniyi AG, Ighalo JO, Onifade DV (2019) Production of Biochar from Elephant Grass (Pernisetum purpureum) using an Updraft Biomass Gasifier with Retort Heating. Biofuels, 12(10): 1283 - 1290.

[21] Kariper İA (2015) Optical and Structural properties of CrSe Thin Film with Chemical Bath Deposition. Journal of Non-Oxide Glasses 7(3): 37

[22] Nwabue FI, Okafor EN (1992) Studies on the Extraction and Spectrophotometric determination of Ni(II), Fe(II) and V(IV) with bis(4-hydroxypent-2-ylidine)diaminoethane. Talanta (3): 273 - 280.

[23] Nwabue FI, Oroke EC, Onah DU, Nworie FS, Ikelle II (2024) Effect of Order of Reagents Addition on Optical and Structural Properties of CdS Quantum Dot Prepared by Chemical Bath Deposition Technique. Iraqi Journal of Science 65(3): 1172-1187.

[24] Chaudhari MN, Ahirrao, RB, Bagul SD (2021) Thin film Deposition Methods: A Critical Review. International Journal for Research in Applied Science & Engineering Technology (IJRASET) 9(6): 2321-9653

[25] Janarthanan B, Thirunavukkarasu C, Maruthamuthu S, Manthrammel MA, Shkir M, AlFaify S, Selvakumar M, Reddye VRM, Park C (2021) Basic deposition methods of thin films. Journal of Molecular Structure 1241: 130606.

[26] SenthilKumar P, Ramalingam S, Abhinaya RV, Kirupha SD, Vidhyadevi T, Sivanesan S (2012) Adsorption Equilibrium, Thermodynamics, Kinetics, Mechanism and Process Design of Zinc(II) ions onto Cashew Nut Shell. Can. J. Chem. Eng 90: 973 - 982.

[27] Altun T, Ecevit H, Kar Y, Çiftçi B (2021) Adsorption of Cr(VI) onto Cross-linked Chitosan-almond Shell Biochars: Equilibrium, Kinetic, and Thermodynamic studies. Journal of Analytical Science and Technology 12: 38.

[28] Vanaraj S, Cindhu B, Preethi K, Sathiskumar S, Mohammed AA, Samy S, Chellasamy P (2022) Ultrasonication-enhanced green synthesis of silver nanoparticles using Barleria buxifolia leaf extract and their possible application, Artificial Cells, Nanomedicine, and Biotechnology, 50:1, 177-187

[29] Bayisa YM, Bullo TA, Akuma DA (2021) Chromium removal from Tannery effluents by Adsorption process via Activated Carbon chat stems (Catha edulis) using Response Surface Methodology. BMC Research Notes 14: 431.

[30] Hamzah Z and Shuhaimi SNA (2018) Biochar: Effects on Crop growth. IOP Conf. Series: Earth and Environmental Science 215: 012011.

[31] Najib S, Bakan F, Abdullayeva N, Bahariqushchi R, Kasap S, Franzò G, Sankir M, Sankir N D, Mirabella S, Erdem E (2020) Tailoring morphology to control defect structures in ZnO electrodes for highperformance supercapacitor devices. Nanoscale 12: 16162.

[32] Udofia KI, Ikhioya IL, Okoli DN, Ekpunobi AJ (2023) Impact of doping on the physical properties of PbSe chalcogenide material for photovoltaic application Asian Journal of Nanoscience and Materials 6(2): 135 - 147.

[33] Arikpo JU, Onuu MU (2020) Optical and electrical characterization of microwave power system chemical vapour deposited (MPS-CVD) grapheme on Ni electroplated Cu foil at varying temperature. Vacuum 182: 109 – 767.

[34] Adamo T (2021) Understanding Raman Spectroscopy principles and theory. Traces Centre 5: 01.

[35] Chen M, Bao C, Hua D, Jina X (2019) Facile and low-cost fabrication of ZnO/biochar nanocomposites from jute fibers for efficient and stable photodegradation of methylene blue dye. Huang Q. Journal of Analytical and Applied Pyrolysis 139: 319–332.

[36] Ashok A, Regmi G, Romero-Nunez A, Solis-Lopez M, Velumani S Castaneda H (2020) Comparative studies of CdS thin films by Chemical Bath Deposition Techniques as a buffer layer for Solar cell applications. Journal of Materials Science: Materials in Electronics 31(2): 7499 – 7518.

[37] Raj ILP, Christy AJ, Prabu RD, Chidhambaram N, Shki M, AlFaify S, Khan A (2020) Significance of Ni doping on Structure-morphology-photoluminescence, Optical and Photocatalytic activity of CBD grown ZnO nanowires for Opto-photocatalyst applications. Inorganic Chemistry Communications 119:108082.

[38] Roguai S, Djelloul AA (2020) Structural and Optical properties of Cu-doped ZnO films prepared by spray pyrolysis. Applied Physics A 26: 122.

[39] Minhas H, Deepak KD, Kumar A (2019) Preparation, Characterization and Electromagnetic Interference Shielding Effect of Ni-doped ZnO Thin Films. Mater. Res. Express 6(10):

[40] Bagheri A, Abu-Danso E, Iqbal J, Bhatnagar A (2020) Modified Biochar from Moringa seed powder for the removal of Diclofenac from Aqueous solution. Environmental Science and Pollution Research 27: 7318.

[41] Ahmad T, Khan MAM, Kumar S, Ahmed M, Shahabuddin M, Alhazaa AN (2016) CdS quantum dots: growth, microstructural, optical and electrical characteristics. Appl. Phys. B 122:179.

[42] Hamza UD, Nasri NS, Amin NS, Mohammed J, Zain HM (2016) Characteristics of Oil palm shell Biochar and Activated Carbon prepared at different carbonization times. Desalination and Water Treatment 57(17): 7999 - 8006.

[43] Devens KU, Neto SP, Oliveira DLA, Gonçalves MS (2018) Characterization of Biochar from Green Coconut Shell and Orange Peel Wastes. Rev.Virtual Quim 10(2): 288 - 294.

[44] Mian MM, Guijian L (2018) Recent progress in biochar supported photocatalysts: Synthesis, role of biochar, and applications. RSC Adv 8: 14237 - 14248.

[45] Wang P, Tang L, Wei X, Zeng G, Zhou Y, Deng Y, Wang J, Xie Z, Fang W (2017) Synthesis and application of Iron and Zinc doped Biochar for removal of p-nitrophenol in wastewater and assessment of the influence of co-existed Pb(II). Applied Surface Science 392: 391.

[46] Eltaweil AS, Abdelfatah AM, Hosny M, Fawzy M (2022) Novel Biogenic Synthesis of a Ag@Biochar Nanocomposite as an Antimicrobial Agent and Photocatalyst for Methylene Blue Degradation.ACS Omega 7: 8046 - 8059.

[47] Nworie FS, Oroke EC, Ikelle II, Nworu JS (2020) Equilibrium and Kinetic Studies for The Adsorptive Removal of Lead (II) Ions from Aqueous Solution Using Activated Plantain Peel Biochar. Acta Chemica Malaysia (ACMY) 4(1): 2576.

[48] Chakraborty R., Asthana A., Singh A. K., Jain B., Abu BHS (2020) Adsorption of heavy metal ions by various low-cost adsorbents: A review. International Journal of Environmental Analytical Chemistry 102(2): 342 - 379.

[49] Norbert OR, Marwa E, Ahmed E, Manabu F, Sekiguchi H, Hassan S (2022) Novel nano-biosorbent materials from thermal catalytic degradation of green pea waste for cationic and anionic dye decolorization. Biomass Conversion and Biorefinery, https://doi.org/10.1007/s13399-022-03299-y

[50] Gürkan EH, İlyas B (2022) Adsorption of Copper and Zinc onto novel Ca-alginate-biochar composite prepared by biochars produced from pyrolysis of groundnut husk. International Journal of Phytoremediation 24(13): 1350 - 1363.

[51] Li X., Zhu X, Jin K, Yang D (2020) Study on structural and optical properties of Mn-doped ZnO thin films by sol-gel method Optical Materials 100: 109657.

[52] Ebelegi NA, Inengite AK, Ayawei N, Wankasi D (2017) Modeling of Adsorption Isotherms for Methylene Blue Sorption onto Fly Ash Modified with Hydrochloric Acid. Journal of Chemical Science and Technology 6 (1): 1 - 20.

[53] Agrafioti E., Kalderis D., Diamadopoulos E (2014) Arsenic and chromium removal from water using biochars derived from rice husk, organic solid wastes and sewage sludge. Journal of Environmental Management 133: 309 - 314.

[54] Nworie FS, Nwabue FIk., Ikelle II, Ogah AO, Elom N, Illochi NO, Itumoh EJ, Oroke CE (2018) Activated Plantain Peel Biochar As Adsorbent For Removal of Zinc(II) Ions From Aqueous Solution: Equilibrium and Kinetics Studies. Journal of Turkish Chemical Society A 5(3): 1257 - 1270.

[55] Nworie FS, Oti WO, Nwali U (2021) Modeling and analysis of batch extraction process for efficient removal of cadmium and pathogens from aqueous solution using modified plantain peel biochar. Wireless Sensor Network 157: 1